High-speed nano-imaging using dynamic mode AFM: A MAP detection approach

Naveen Kumar*, Govind Saraswat†, Pranav Agarwal†, Aditya Ramamoorthy* and Murti Salapaka†
*Dept. of Electrical and Computer Engineering
Iowa State University, Ames, IA 50010
Email: nk3,adityar@iastate.edu
†Dept. of Electrical and Computer Engineering
University of Minnesota, Minneapolis, MN 55455
Email: saras006,agar0108,murtis@umn.edu

***Abstract*—Nano-imaging has played a vital role in biology, chemistry and physics as it enables interrogation of material with sub-nanometer resolution. Primary means of achieving such atomic scale interrogation of matter are based on the principles of atomic force microscopy (AFM) and scanning tunneling microscopy (STM). However, current nano-imaging techniques are too slow to be useful in the high speed applications of interest such as studying the evolution of certain biological processes over time that involve very small time scales. In this work, we present a high speed one-bit imaging technique using dynamic mode AFM with a high quality factor cantilever. We model the high quality factor cantilever system using a Markovian model which incorporates the inherent system memory due to the inter-symbol interference and the cantilever state. Next, we pose the imaging problem as one of finding the maximum a posteriori (MAP) symbol detector for this model. This is solved by adapting the BCJR algorithm for our channel model. Furthermore, we propose an improved MAP symbol detector that incorporates a learned prior from the previous scan line while detecting the features on the current scan line. Experimental results demonstrate that our proposed algorithm provides significantly better image resolution compared to current nano-imaging techniques at high scanning speed.**

I. Introduction

The technologies of nano-interrogation and nano-imaging have resulted in major breakthroughs in various fields, including biology, chemistry, physics and medicine. The ability to see things at the level of a few nanometers is critical in many of these domains. This has been made possible through instruments such as atomic force microscopes (AFM), scanning tunneling microscopes (STM) etc. Current nanoimaging technology though useful, suffers from severe speed limitations. Current techniques essentially rule out imaging chemical and biological processes that evolve at time scales that are typically faster than the imaging speed, e.g. movement of kinesins along microtubules. Moreover, in many cases we are interested in fast imaging of samples that are of the order of a few square centimeters or even higher in some applications e.g., fault detection in semiconductor fabrication.

AFM plays a vital role in controlling, manipulating and interrogating matter at the atomic scale. For example, many applications of AFM cantilevers in biological sciences involve cutting DNA strands [4] and investigating the activity of RNA polymerase [3]. In nano-imaging, the samples, to be imaged, are mostly soft which leads to the use of dynamic mode AFM. In the dynamic mode operation, the cantilever is forced sinusoidally using a dither piezo. The oscillating cantilever gently taps the sample and thus the lateral forces are reduced which decreases the sample wear [9]. The amplitude of the cantilever oscillation changes due to tip-sample interaction. The amplitude of the first harmonic of the cantilever oscillation is obtained from the cantilever deflection signal in amplitude modulation method. This amplitude signal can be used to image samples and referred as amplitude imaging [1]. In [7], the cantilever-observer architecture is introduced which removes the effect of dither and provides a better way to image samples. The innovation signal is obtained through the output of the cantilever-observer architecture. The root mean square of the innovation signal gives a fast way to image samples and referred as root mean square imaging [8]. But current imaging techniques are too slow to be useful in high fidelity imaging of chemical and biological processes that evolve at fast time scales.

In [6], we have considered the development of a high-density data storage device using dynamic mode AFM. Here, the information is encoded using nanoscale topographic profiles, e.g., '1' - indentation and '0' - no indentation. In order to enable high access speeds, one needs to be able to infer the underlying bit pattern at a fast rate. We have shown that under practically validated modeling assumptions, the entire system can be viewed as a communication system. Moreover, one can map the overall problem of detecting the presence/ absence of the bits as one of Bayesian inference over factor graphs. The bit detection problem requires us to decide whether or not a single topographic feature exists on the sample. This bit detection problem can be posed as maximum likelihood sequence detection (MLSD) problem which can be solved using Viterbi decoding [6]. Furthermore, in the data storage application one can choose the topographic features and sample material. In contrast, high-fidelity imaging requires us to figure out the height and shape of the underlying sample to within 8-bit precision (for example). Moreover, an imaging technique should be general enough to operate under various sample types. Thus, the nano-imaging problem is significantly richer and more complicated.

In this paper, we consider one-bit imaging, i.e., we wish to detect the presence/absence of a feature. This will be

generalized to multi-bit imaging in future. In one-bit imaging technique, the raster scan is used for imaging which means that the image is subdivided into a sequence of horizontal scan lines and each scan line is imaged using the AFM imaging scanner. Each scan line consists of bit-pixels which can be either '0' or '1'. This problem of imaging is similar to the problem of detecting the presence/ absence of the bits in probe based data storage system. It allows us to use the channel model developed in [6] for imaging purposes. But it is important to note that Viterbi detector developed in [6] cannot be used for imaging purposes. Viterbi detector assumes equiprobable prior on the input bit sequence which is not true in imaging scenarios as the images will have non-equiprobable priors on input depending upon the features present in the image. This demands designing a detection strategy for nano-imaging applications which can incorporate non-equiprobable priors. Next, the imaging of chemical and biological processes, that evolve at fast time scales, drives the need for high scan rate imaging. But the feature detection at high scan rates becomes quite challenging as the tip-sample interaction duration for each feature decreases with a increase in the scan rate. Thus, the main challenge in nano-imaging is to develop an imaging technique which can incorporate the non-equiprobable priors and provide good resolution at very high scan speeds.

Main Contributions: In this paper, a one-bit imaging technique using dynamic mode operation with a high quality factor cantilever is presented. The cantilever-based nano-imaging system for the one-bit imaging is modeled as an appropriate communication channel model which incorporates the inherent system memory due to the inter-symbol interference and the cantilever state. We first develop the maximum a posteriori (MAP) symbol detector for this channel model. The MAP symbol detection problem is solved by adapting the BCJR algorithm [2] for our channel model. Next, we propose an improved MAP symbol detector that incorporates a learned prior from the previous scan line while detecting the features on the current scan line. Experimental results demonstrate that our proposed algorithm provides significantly better image resolution compared to current imaging techniques at high scanning speed.

The paper is organized as follows. Section II presents the communication channel model for the cantilever-based nano-imaging system and deals with designing an imaging algorithm using MAP symbol detector. Section III reports results from experiments. Section IV summarizes the main findings of this paper and provides the conclusions and future work.

II. Channel model and imaging algorithm

The cantilever based nano-imaging system can be modeled as a communication channel as shown in Figure 1 [6]. The components of this model are explained below in detail.

Shaping Filter ($b(t)$): The model takes as input the bit-pixel sequence $(a_0,\ a_1 \dots\ a_{N-1})$ from the image sample where $a_k, k = 1, \dots, N-1$ can be '0' or '1'. In the nano-imaging context, '0' refers to the topographic profile being *low* (absence of feature in the image) and '1' refers to the topographic profile being *high* (presence of feature in the image). Each bit-pixel has a duration of T seconds. This duration can be found based on the length of the topographic feature present in image sample and the speed of the image scanner. The height of the topographic feature, when the bit-pixel is '1', is denoted by A. The cantilever interacts with the sample by gently tapping it when it is high. When the sample is low, typically no interaction takes place. We model the effect of the sample height using a filter with impulse response $b(t)$ (shown in Figure 1) that takes as input, the input bit-pixel impulse train $a(t) = \sum_{k=0}^{N-1} a_k \delta(t - kT)$. The output of the filter is given by $\breve{a}(t) = \sum_{k=0}^{N-1} a_k b(t-kT)$ which is high/low when the corresponding bit is '1'/'0'.

Nonlinearity Block (ϕ): The nonlinearity block models the tip-sample interaction forces. The nonlinearity block output is modeled as a sequence of impulsive force inputs to the cantilever [6]. The cantilever oscillates at frequency f_c which means that in each cantilever cycle of duration $T_c (= 1/f_c)$, the cantilever hits the sample at most once if the sample is high during a time T_c. In each high bit duration T, the cantilever hits the sample q times (i.e. $T \approx qT_c$) with varying interaction magnitudes. Therefore, for N bits, the output of the nonlinearity block is given by, $\tilde{a}(t) = \sum_{k=0}^{Nq-1} \nu_k(\bar{a}) \delta(t - kT_c)$, where ν_k denotes the magnitude of the k^{th} impact of the cantilever on the sample. The strength of the impulsive force inputs are dependent on previous impulsive hits; precisely because the previous interactions affect the amplitude of the oscillations that in turn affect how hard the hit is at a particular instant of time. A Markov model on the sequence of impact magnitudes for a single bit-pixel duration is given by [6],

$$\bar{\nu}_k = \bar{\mathfrak{G}}(a_k, a_{k-1}, \dots, a_{k-m}) + \bar{\mathfrak{b}}_k, \tag{1}$$

where $\bar{\mathfrak{G}}(a_k, a_{k-1}, \dots, a_{k-m})$ is a function of current and last m bits, m denotes the inherent memory of the system, $\bar{\nu}_k = [\nu_{kq}\ \nu_{kq+1} \dots \nu_{(k+1)q-1}]^T$ and $\bar{\mathfrak{b}}_k$ is a zero mean i.i.d. Gaussian vector of length q.

Channel Response ($\Gamma(t)$): $\Gamma(t)$ is the impulse response of the cantilever-observer system described in [6]. The cantilever-observer system provides a better way of real-time imaging the samples with scan speed quite faster than conventional methods [8].

Channel Noise ($n(t)$): The measurement noise (from the imprecision in measuring the cantilever position) and thermal noise (from modeling mismatches) can be modeled by a single zero mean white Gaussian noise process ($n(t)$) with power spectral density equal to V.

The continuous output $e(t)$ of the channel model named as innovation signal is,

$$e(t) = \sum_{k=0}^{Nq-1} \nu_k(\bar{a}) \Gamma(t - kT_c) + n(t) = s(t, \bar{\nu}(\bar{a})) + n(t),$$

where $s(t, \bar{\nu}(\bar{a})) = \sum_{k=0}^{Nq-1} \nu_k(\bar{a}) \Gamma(t - kT_c)$ and $\bar{\nu}(\bar{a}) = (\nu_0(\bar{a}),\ \nu_1(\bar{a}) \dots\ \nu_{Nq-1}(\bar{a}))$. The sequence of impact values $\bar{\nu}_k$ is assumed to follow a Markovian model as explained above, $\Gamma(t)$ is the channel impulse response and $n(t)$ is a zero mean white Gaussian noise process.

A. Discretized Channel Model

It can be shown that the output of a whitened matched filter shown in Figure 1 provides the sufficient statistics

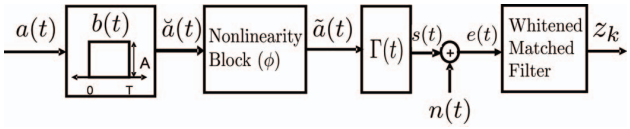

Fig. 1. Discretized channel model with whitened matched filter

for our channel model [6]. We shall denote the discretized output of whitened matched filter as z_k, such that $z_k = \sum_{k_1=0}^{I} \nu_{k-k_1}(\bar{a}) h_{k_1} + n_k$, where the filter $\{h_k\}_{k=0,1,\ldots,I}$ denotes the effect of the whitened matched filter and the sequence $\{n_k\}$ represents Gaussian noise with variance V [6].

Let $\bar{z}_k$ be the received output vector corresponding to the k^{th} input bit-pixel i.e. $\bar{z}_k = [z_{kq}\ z_{kq+1} \ldots z_{(k+1)q-1}]^T$ and $\bar{z}_0^{k-1} = [\bar{z}_0^T\ \bar{z}_1^T \ldots \bar{z}_{k-1}^T]^T$. In our model, the channel is characterized by a finite impulse response of length I i.e. $h_k = 0$ for $k < 0$ and $k > I$. In this work we assume that $I \leq m_I q$ i.e. the inter-symbol-interference (ISI) length in terms of q hits is equal to m_I. Let m be the inherent memory of the system (see (1)). The length of channel response m_I is known and the value of m can be found by the method described in [6]. The received output vector $\bar{z}_k$ can now be written as,

$$\bar{z}_k = \begin{pmatrix} h_I & . & . & h_0 & 0 & . & . & 0 \\ 0 & h_I & . & . & h_0 & 0 & . & 0 \\ . & . & . & . & . & . & . & . \\ 0 & . & . & 0 & h_I & . & . & h_0 \end{pmatrix} \begin{pmatrix} \nu_{kq-I} \\ \nu_{kq-I+1} \\ \vdots \\ \nu_{(k+1)q-1} \end{pmatrix} + \bar{n}_k$$

$$= H\bar{\nu}_{k-m_I}^k + \bar{n}_k$$

where $\bar{\nu}_k = [\nu_{kq}\ \nu_{kq+1} \ldots \nu_{(k+1)q-1}]^T$, $\bar{\nu}_{k-m_I}^k = [\bar{\nu}_{k-m_I}^T \ \ldots\ \bar{\nu}_k^T]^T$, $\bar{n}_k = [n_{kq}\ n_{1+kq} \ldots n_{(k+1)q-1}]^T$.

In [6], the dependency graph on the concerned quantities is constructed and $f(\bar{z}_k|\bar{a}, \bar{z}_0^{k-1})$ is simplified as,

$$f(\bar{z}_k|\bar{a}, \bar{z}_0^{k-1}) = f(\bar{z}_k|a_{k-m-m_I}^k, \bar{z}_{k-m_I}^{k-1}). \tag{2}$$

where $f()$ denotes the p.d.f, m is the inherent system memory and m_I is the inter-symbol-interference (ISI) length in terms of bits. By defining a state $S_k = a_{k-m-m_I+1}^k$, this can be further expressed as $f(\bar{z}_k|S_k, S_{k-1}, \bar{z}_{k-m_I}^{k-1})$.

B. BCJR Algorithm

The a posteriori probability (APP) of a symbol, a_k is defined as, $APP(a_k) = f(a_k|\bar{z})$. In MAP symbol detection, the symbol a_k is found which maximizes the $APP(a_k)$. We now derive MAP symbol detector for our channel model. The symbols ζ', ζ and ζ'' denote the past, current and future states respectively where the state at kth time instant is defined as $S_k = a_{k-m-m_I+1}^k$. In BCJR algorithm, $f(a_k, \bar{z})$ is computed instead of $f(a_k|\bar{z})$,

$$\begin{aligned} f(a_k, \bar{z}) &= \sum_{\zeta'} f(S_{k-1} = \zeta', a_k, \bar{z}) \\ &= \sum_{\zeta'} \alpha_{k-1}(\zeta').\gamma_k(\zeta', \zeta).\beta_k(\zeta) \end{aligned}$$

where $\alpha_{k-1}(\zeta') = f(S_{k-1} = \zeta', \bar{z}_0^{k-1})$, $\gamma_k(\zeta', \zeta) = f(\bar{z}_k|S_k = \zeta, S_{k-1} = \zeta', \bar{z}_{k-m_I}^{k-1})P(a_k)$ and $\beta_k(\zeta) = f(\bar{z}_{k+1}^{N-1}|S_k = \zeta, \bar{z}_{k-m_I+1}^{k})$.

It should be noted that the pair $(S_{k-1} = \zeta', a_k)$ completely determines state S_k. The variables $\alpha_k(\zeta)$ and $\beta_k(\zeta)$ has recursive structure,

$$\begin{aligned} \alpha_k(\zeta) &= \sum_{\zeta'} \alpha_{k-1}(\zeta').\gamma_k(\zeta', \zeta) \\ \beta_k(\zeta) &= \sum_{\zeta''} \beta_{k+1}(\zeta'').\gamma_{k+1}(\zeta, \zeta'') \end{aligned}$$

Typical Initialization for $\alpha_k(\zeta)$ and $\beta_k(\zeta)$ variables is,

$$\alpha_{-1}(\zeta) = \begin{cases} 1, \text{if } \zeta = 0 \\ 0, \text{if } \zeta \neq 0 \end{cases} \quad \text{and } \beta_{N-1}(\zeta) = \begin{cases} 1, \text{if } \zeta = 0 \\ 0, \text{if } \zeta \neq 0 \end{cases}$$

In implementation, the forward and backward recursions are done in log domain. The recursion equations in log domain are as follows,

$$\begin{aligned} \log(\alpha_k(\zeta)) &= \log \sum_{\zeta'} e^{\log(\alpha_{k-1}(\zeta')) + \log(\gamma_k(\zeta', \zeta))} \\ \log(\beta_k(\zeta)) &= \log \sum_{\zeta''} e^{\log(\beta_{k+1}(\zeta'')) + \log(\gamma_{k+1}(\zeta, \zeta''))} \\ \log(\gamma_k(\zeta', \zeta)) &= \log(f(\bar{z}_k|S_{k-1} = \zeta', S_k = \zeta, \bar{z}_{k-\zeta_I}^{k-1})) \\ &\quad + \log(P(a_k)) \end{aligned}$$

In above equation, the term $f(\bar{z}_k|S_{k-1} = \zeta', S_k = \zeta, \bar{z}_{k-\zeta_I}^{k-1})$ can be computed by making an assumption that $f(\bar{z}_{k-m_I}^k|S_k, S_{k-1})$ is Gaussian distributed [6], i.e.,

$$f(\bar{z}_{k-m_I}^k|S_k = \zeta, S_{k-1} = \zeta') \sim N(\bar{\mu}(\zeta, \zeta'), \mathcal{C}(\zeta, \zeta')),$$

where $\bar{\mu}(\zeta, \zeta')$ is the mean vector and $\mathcal{C}(\zeta, \zeta')$ is the covariance matrix. Now the term $\log(f(\bar{z}_k|S_{k-1} = \zeta', S_k = \zeta, \bar{z}_{k-\zeta_I}^{k-1}))$ can be computed as ,

$$\begin{aligned} &\log(f(\bar{z}_k|S_k = \zeta, S_{k-1} = \zeta', \bar{z}_{k-m_I}^{k-1})) \\ &= \log(\frac{f(\bar{z}_{k-m_I}^k|S_k = \zeta, S_{k-1} = \zeta')}{f(\bar{z}_{k-m_I}^{k-1}|S_k = \zeta, S_{k-1} = \zeta')}) \\ &= -\frac{1}{2}\log\frac{|\mathcal{C}(\zeta, \zeta')|}{|c(\zeta, \zeta')|} - \frac{1}{2}(\bar{z}_{k-m_I}^k - \bar{\mu}(\zeta, \zeta'))^T \\ &\cdot \mathcal{C}(\zeta, \zeta')^{-1}(\bar{z}_{k-m_I}^k - \bar{\mu}(\zeta, \zeta')) + \frac{1}{2}(\bar{z}_{k-m_I}^{k-1} \\ &- \bar{\lambda}(\zeta, \zeta'))^T c(\zeta, \zeta')^{-1}(\bar{z}_{k-m_I}^{k-1} - \bar{\lambda}(\zeta, \zeta')) \end{aligned}$$

where $c(\zeta, \zeta')$ is the upper $m_I q \times m_I q$ principal minor of $\mathcal{C}(\zeta, \zeta')$ and $\bar{\lambda}(\zeta, \zeta')$ collects the first $m_I q$ elements of $\bar{\mu}(\zeta, \zeta')$. Using above results, $\log(f(a_k, \bar{z}))$ can be computed as,

$$\log(f(a_k, \bar{z})) = \log \sum_{\zeta'} e^{\log(\alpha_{k-1}(\zeta')) + \log(\gamma_k(\zeta', \zeta)) + \log(\beta_k(\zeta))}$$

The log-likelihood ratio can be computed using the above results,

$$\begin{aligned} L(a_k) &= \log\frac{f(a_k = 0|\bar{z})}{f(a_k = 1|\bar{z})} \\ &= \log(f(a_k = 0, \bar{z})) - \log(f(a_k = 1, \bar{z})) \end{aligned}$$

Algorithm 1 : BCJR Imaging Algorithm.

1) Decode the first scan line with the equiprobable prior on the input.
2) Update the prior and use it for decoding the second scan line.
3) Sequentially keep updating the prior and decode the successive scan lines.

The forward and backward recursions given above can be used to find $L(a_k)$. The decision rule for finding the bit is given by, $L(a_k) \lessgtr 1, 0$.

C. Imaging Algorithm

The raster scan is used for imaging which means that the image is subdivided into a sequence of horizontal scan lines. The features in the images are assumed to be spatially continuous which means that the image does not change much between two consecutive scan lines. This information can be incorporated in the BCJR algorithm to provide better imaging. The advantages of using BCJR algorithm are twofold; the first is that the log-likelihood ratios obtained from decoding one scan line can directly give probabilistic prior on each symbol in the scan line and the second is that this probabilistic prior on each symbol can be used in computing the term $\gamma_k(\zeta', \zeta)$ while decoding the next scan line. It should be noted that the current scan line can be decoded using the probabilistic prior obtained from previous scan line. But in the start of imaging, no information about the first scan line is available which forces us to use the equiprobable prior on input in decoding the first scan line. Using the above ideas, the BCJR imaging algorithm is summarized in Algorithm 1.

The current state of art techniques include a) Amplitude imaging - this imaging is done through envelope of deflection signal [1] b) Root mean square imaging - the root mean square of the innovation signal is used for this imaging [8] and (c) LMP imaging - locally most powerful test is used on the innovation signal in this case to reconstruct the binary image [5].

III. Experimental Results

We performed experiments for one-bit imaging with a cantilever with resonant frequency $f_0 = 74.73$ KHz and quality factor $Q = 140.68$. A freshly cleaved mica sheet is used as an imaging sample. The experiments were performed on Multimode AFM, from Veeco Instruments. We have performed the imaging at different scan rate. One pixel in the image corresponds to high or low topographic profile. We considered the test pattern shown in Figure 2(a), that is of dimension $2.7\ \mu\text{m} \times 10\mu\text{m}$. In first set of experiments, we took the scan rate such that each pixel remains high or low for $120\ \mu$sec which means cantilever will hit around 8 times if the topographic profile is high. Each line scan of size $10\ \mu$m with 512 pixels resolution will get done in $\frac{1}{74.73\times 10^3} \times 8 \times 512$ seconds. The scan rate in this case will be $10/8/512/74.73 \times 10^3 = 182.44\ \mu$m/sec. In Figure 2, the performance of current state of the art techniques is compared with our proposed technique at $182.44\ \mu$m/sec

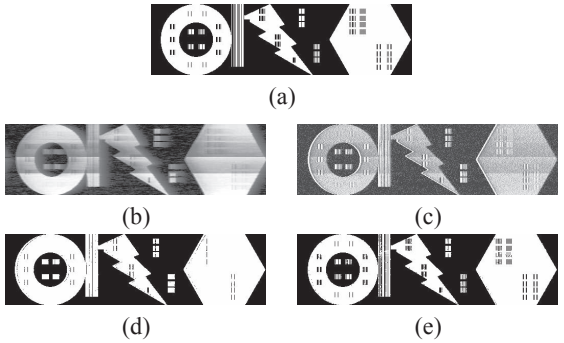

Fig. 2. Comparison of imaging techniques at a scan rate of $182.44\ \mu$m/sec. (a) Reference test pattern, (b) Amplitude imaging (c) Root mean square imaging (d) LMP imaging (e) BCJR Imaging

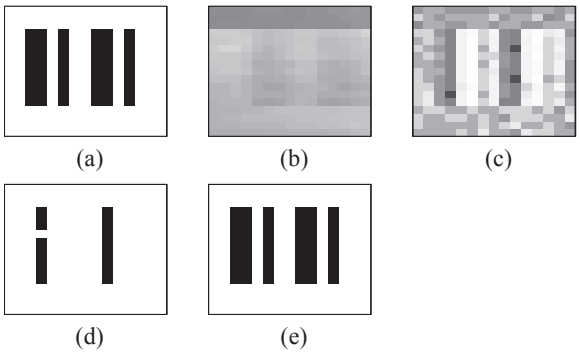

Fig. 3. Comparison of the feature resolution provided by different techniques at scan rate of $182.44\ \mu$m/sec. A zoomed image is provided for facilitating visual comparison. (a) Reference test pattern, (b) Amplitude imaging (c) Root mean square imaging (d) LMP imaging (e) BCJR Imaging

imaging speed. In order to see the improvement provided by our method, we have zoomed in the images and shown the spatial features in Figure 3. In Figure 3, it is clearly seen that our algorithm cleanly resolves all the spatial features present in the image whereas other imaging techniques cannnot. It is evident that the proposed technique has much better fidelity providing better resolution even at high scan speeds.

In another set of experiments, we took the scan rate such that each pixel remains high or low for $80\ \mu$sec which means cantilever will hit around 5 times if the topographic profile is high. In this case, the scan rate is given by $10/5/512/74.73 \times 10^3 = 291.91\ \mu$m/sec. The images at $291.91\ \mu$m/sec scan rate are shown in Figure 4. The zoomed spatial features at this scan rate are shown in Figure 5. In this case, our proposed technique resolves the features in a better manner as compared to other imaging techniques. We have even done the experiments at very high scan rate $729.78\ \mu$m/sec. The images at $729.78\ \mu$m/sec scan rate are shown in Figure 6. The zoomed spatial features at this scan rate are shown in Figure 7. It can be observed that our proposed techniques is not able to resolve the high spatial frequency features in the image but it does resolve low spatial frequency features whereas other imaging methods again completely fail. In nutshell, our proposed technique outperforms all the current state of art imaging techniques.

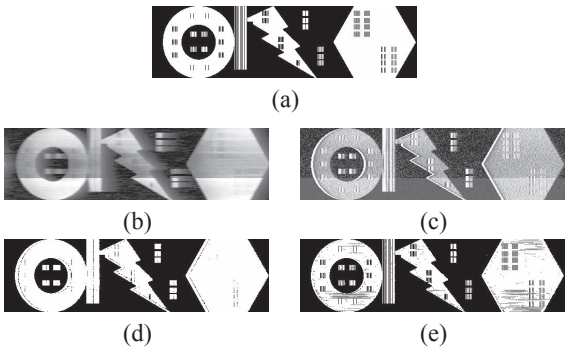

Fig. 4. Comparison of imaging techniques at a scan rate of 291.91 μm/sec. (a) Reference test pattern, (b) Amplitude imaging (c) Root mean square imaging (d) LMP imaging (e) BCJR Imaging

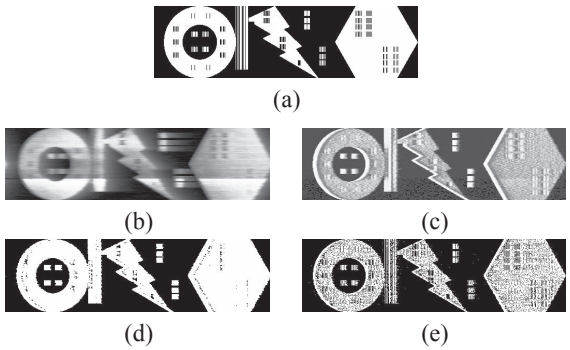

Fig. 6. Comparison of imaging techniques at a scan rate of 729.78 μm/sec. (a) Reference test pattern, (b) Amplitude imaging (c) Root mean square imaging (d) LMP imaging (e) BCJR Imaging

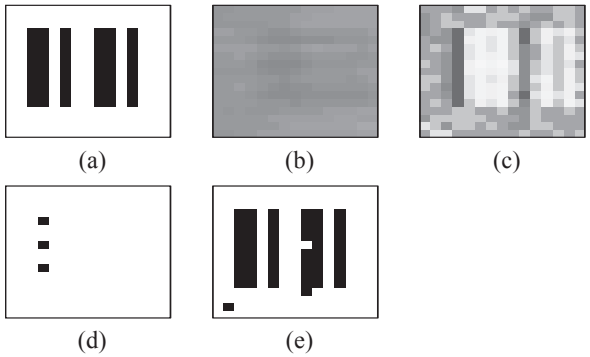

Fig. 5. Comparison of the feature resolution provided by different techniques at scan rate of 291.91 μm/sec. A zoomed image is provided for facilitating visual comparison. (a) Reference test pattern, (b) Amplitude imaging (c) Root mean square imaging (d) LMP imaging (e) BCJR Imaging

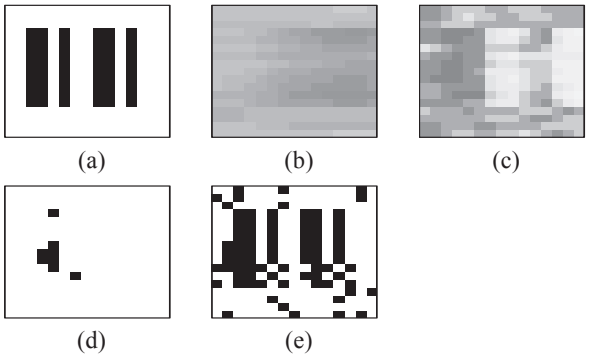

Fig. 7. Comparison of the feature resolution provided by different techniques at scan rate of 729.78 μm/sec. A zoomed image is provided for facilitating visual comparison. (a) Reference test pattern, (b) Amplitude imaging (c) Root mean square imaging (d) LMP imaging (e) BCJR Imaging

IV. Conclusions and future work

We have presented the channel model for the cantilever based nano-imaging system. We have developed the maximum a posteriori (MAP) symbol detector which does take into account the image prior while detecting the features on the image. The MAP symbol detection problem is solved by adapting the BCJR algorithm. We further proposed the imaging algorithm for the raster scan imaging which incorporates the input prior from previous line scan while detecting the features on the current line scan. Experimental results corroborate the analysis of the detector, demonstrate that our proposed algorithm does provide better image resolution compared to current imaging techniques at high scanning speed. In future, these techniques will enable video rate imaging of molecular scale phenomenon. This will address the issue of being able to visualize and understand dynamics at the nano-scale.

Currently one-bit imaging is proposed in this paper. This work can be extended for multi-level imaging where not only the absence or presence of topographic profile is specified but the height of topographic profile can also be found. This kind of information is quite useful in finding the structure and movement of a biological process.

References

[1] T. Ando, N. Kodera, E. Takai, D. Maruyama, K. Saito, and A. Toda. A high-speed atomic force microscope for studying bilological macromolecules. *Proceedings of National Academy of Science*, 98(22):034106, 2001.

[2] L. Bahl, J. Cocke, F. Jelinek, and J. Raviv. Optimal decoding of linear codes for minimizing symbol error rate (corresp.). *Information Theory, IEEE Transactions on*, 20(2):284 – 287, mar 1974.

[3] S. Kasas, N. H. Thomsona, B. L. Smith, H. G. Hansma, et al. Escherichia coli rna polymerase activity observed using atomic force microscopy. *Biochemistry*, 36(3):461 – 468, 1997.

[4] D. O. Koralek, W. F. Heinz, M. D. Antonik, A. Baik, and J. H. Hoh. Probing deep interaction potentials with white-noise-driven atomic force microscope cantilevers. *IEEE T. Instrum. Meas.*, 76:2952, 2000.

[5] N. Kumar, P. Agarwal, A. Ramamoorthy, and M. Salapaka. Channel modeling and detector design for dynamic mode high density probe storage. In *42nd Conference on Information Sciences and Systems*. IEEE, 2008.

[6] N. Kumar, P. Agarwal, A. Ramamoorthy, and M. Salapaka. Maximum likelihood sequence detector for dynamic mode high density probe storage. *IEEE Transactions on Communication*, 58(6), June 2010.

[7] D. R. Sahoo, A. Sebastian, and M. V. Salapaka. Harnessing the transient signals in atomic force microscopy. *International Journal of Robust and Nonlinear Control, Special Issue on Nanotechnology and Micro-biology*, 15:805–820, 2005.

[8] D.R. Sahoo, P. Agarwal, and M.V. Salapaka. Transient force atomic force microscopy: A new nano-interrogation method. In *American Control Conference, 2007. ACC '07*, pages 2135 –2140, 9-13 2007.

[9] Q. Zhong, D. Inniss, K. Kjoller, and V B Elings. Fractured polymer/silica fiber surface studied by tapping mode atomic force microscopy. *Surface Science Letters*, 290:L688–L692, 1993.